Desalination and Water Treatment
www.deswater.com

doi: 10.1080/19443994.2015.1083892

57 (2016) 16943–16954
August

Taylor & Francis
Taylor & Francis Group

Magnetic Fe_3O_4/sepiolite composite synthesized by chemical co-precipitation method for efficient removal of Eu(III)

Shaoming Yu*, Xiguang Liu, Gaojin Xu, Yong Qiu, Leilei Cheng

School of Chemistry and Chemical Engineering, Hefei University of Technology, Hefei 230009, Anhui, China, Tel. +86 551 62901342; Fax: +86 551 62901450; emails: shmyu@hfut.edu.cn (S. Yu), lelchg5@gmail.com (X. Liu), collinscheng@163.com (G. Xu), eyrewang@yeah.net (Y. Qiu), leileicheng555@gmail.com (L. Cheng)

Received 23 February 2015; Accepted 8 August 2015

ABSTRACT

In this study, a novel magnetic Fe_3O_4/sepiolite composite (MFSC) was synthesized via chemical co-precipitation method. The synthesized MFSC was characterized by the several kinds of methods. The characterization results showed that MFSC was composed of Fe_3O_4 nanoparticles on the surface of sepiolite. Moreover, MFSC was used as an adsorbent for the removal of Eu(III) from aqueous solutions. The influences of contact time, pH, ionic strength, and temperature were investigated. The synthesized MFSC had a Langmuir adsorption capacity of 30.85 mg/g at 293 ± 1 K, which was much higher than that of some common and low-cost adsorbents. Ion exchange and surface complexation were the main adsorption mechanisms of Eu(III) adsorption on MFSC. The novel MFSC adsorbent is efficient and economical for Eu(III) removal for its good adsorption characteristic, excellent regeneration property, and high magnetic separation efficiency.

Keywords: Magnetic Fe_3O_4/sepiolite composite; Co-precipitation; Eu(III); Adsorption

1. Introduction

Sepiolite ($Mg_8Si_{12}O_{30}(OH)_4(OH_2)_4{\cdot}8H_2O$) is a hydrated magnesium silicate that widely exists in nature as a fibrous clay mineral [1]. It presents a structure of needle-like particles, which can be described as an arrangement of talc-like layers (two layers of tetrahedral silica and a central octahedral magnesium layer) separated by channels running along the *c*-axis of the particles [2]. The channels measure ~1.06 × 0.37 nm^2 in cross section, which contain "zeolitic water" and some exchangeable Mg^{2+} and Ca^{2+}. The structure properties determine the high specific surface area of sepiolite. Moreover, some isomorphic substitutions in the tetrahedral layer, such as Al^{3+} for Si^{4+}, lead to the negatively charged surface of sepiolite. Therefore, sepiolite is a suitable adsorbent for the removal of harmful metal ions from aqueous solutions [3,4].

However, the pristine sepiolite always contains part of impurities such as calcite, talcum, and quartz, and exists in the form of fiber clusters, leading to the decrease in specific surface area of sepiolite, it is necessary to purify the pristine sepiolite and take some defibered treatment of sepiolite fiber clusters [4]. Another problem encountered in practical wastewater treatment is that it was difficult to isolate and recover of sepiolite from aqueous solutions owing to its small size and low density. The drawbacks of sepiolite restrict the widespread applications of sepiolite in wastewater treatment. In recent years, the application

*Corresponding author.

of magnetic adsorbents in wastewater disposal has received widespread attention due to its convenience and speediness in separation and recovery processes [5–10]. The magnetic adsorbent could be easily separated and recovered from the aqueous solutions at an external magnetic field.

With the development of nuclear industry, a large amount of radioactive contamination is produced in many states and the harmful radionuclides are discharged into the environment or biosphere leads to a serious threat to human beings and animals. For example, exposure to radioactive waste can cause serious diseases, such as diarrhea, spasms, cardiovascular system damage, neurological disorder, leukemia, and even cancers [11]. Therefore, the removal of harmful radionuclides, especially the long-life radionuclides such as the lanthanides and actinides, at the solid–water interface is an important concern in nuclear waste treatment [12]. As an eco-friendly and economical method, the adsorption technique has been employed widely for the removal of radionuclides from large volumes of wastewaters [13–15]. Furthermore, to the best of our knowledge, few researches focus on the adsorption of radionuclides on the magnetic Fe_3O_4/sepiolite composite (MFSC).

As Eu(III) has adsorption properties similar to those of other trivalent lanthanides and actinides, Eu (III) is selected as both a fission product and a homologue of trivalent lanthanides and actinides [16]. In this study, we present a simple approach for synthesizing MFSC via a chemical deposition of Fe_3O_4 nanoparticles onto sepiolite fibers. The physicochemical properties of the synthesized MFSC were carefully characterized by scanning electron microscopy (SEM), X-ray diffraction (XRD), Fourier transform infrared spectroscopy (FT-IR), N_2 adsorption–desorption, vibrating sample magnetometer (VSM), and X-ray photoelectron spectroscopy (XPS). Afterwards, the synthesized MFSC was used for the removal of radionuclide Eu(III) from aqueous solutions. The effects of pH, ionic strength, contact time, and temperature on Eu(III) adsorption on MFSC were investigated. Based on these studies, the adsorption kinetics and thermodynamics of Eu(III) were evaluated.

2. Experimental section

2.1. Reagents and raw material

All chemicals used in the experiments were purchased as analytical purity without any further purification. Double distilled water was used in all experiments. Europium stock solution was prepared from Eu_2O_3 after dissolution, evaporation, and redissolution in perchloric acid. Pristine sepiolite was obtained from Nanyang county (Henan, China) and was milled through a 350-mesh prior to its use in the experiments.

2.2. Preparation of defibered sepiolite

The pristine sepiolite was treated with 1.0 mol/L hydrochloric acid for 2.0 h to remove the calcite, then washed with double distilled water until no chloride was detected with 0.1 mol/L $AgNO_3$. The purified sepiolite was mixed with double distilled water in proportion of 1:20 by weight, and a small amount of sodium hexametaphosphate as dispersant was added into the mixed suspensions, and stirred with a high speed (2,000 rpm) for 2.0 h. Then the mixed suspensions were operated with ultrasonic cleaner for 0.5 h in order to disperse the sepiolite fibers. The defibered sepiolite were dried at 373 ± 1 K for 2.0 h to eliminate the free water and used to synthesize the MFSC.

2.3. Synthesis of MFSC

The MFSC was synthesized by the chemical co-precipitation of Fe^{2+} and Fe^{3+} in alkaline solution in the presence of as-prepared defibered sepiolite [7]. 1.00 g purified sepiolite was transferred to a flask with 200 mL of double distilled water, and the mixed suspensions were operated with ultrasonic cleaner for 0.5 h in order to disperse the sepiolite fibers. Then 1.55 g $FeCl_3{\cdot}6H_2O$ and 0.80 g $FeSO_4{\cdot}7H_2O$ were added into the mixed suspensions under N_2 atmosphere at 343 ± 1 K. A NaOH solution (5.0 mol/L) was added dropwise to precipitate magnetite, then the mixture was adjusted to pH 11.0 and stirred for 1.0 h. The mixture was aged at 343 ± 1 K for 4.0 h and washed with double distilled water until the supernatant pH near to neutral. The obtained sample was dried in a vacuum oven at 353 ± 1 K for 4.0 h. The whole synthesis process of MFSC is schematically illustrated in Fig. 1.

2.4. Physicochemical characterization

The synthesized MFSC was characterized by SEM, XRD, FT-IR, N_2 adsorption–desorption, VSM, and XPS. The morphology of as-synthesized MFSC was studied by a field emission scanner (JEOL JSM-6700F). The crystallographic structures of the MFSC were characterized with XRD patterns on a Rigaku diffractometer (D/max-γB) with a Cu Kα radiation. FT-IR spectra were recorded with a FT-IR spectrometer (Nicolet 67) in the range of 4,000–400 cm^{-1}, using KBr pellets at room temperature. N_2 adsorption–desorption

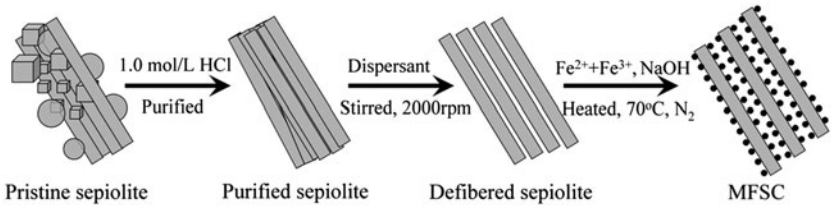

Fig. 1. Synthesis route of MFSC.

isotherms (at 77.3 K) and pore size distribution curves were obtained using a Tristar II 3020 automatic surface area and pore analyzer. The adsorption data were then employed to determine surface area using the Brunauer, Emmett, and Teller (BET). The magnetic measurement was performed in a MPMS-XL SQUID magnetometer at room temperature, and magnetic field was ranging from −20.0 to +20.0 kOe. The XPS measurements were conducted with an ESCALAB250 electron spectrometer.

2.5. Batch adsorption study

The sorption of Eu(III) on MFSC was carried out in 10-mL polyethylene centrifuge tubes under ambient conditions by batch technique. The MFSC content and the concentration of $NaClO_4$ were 0.5 g/L and 0.01 mol/L, respectively. The Eu(III) stock solution including trace quantities of radiotracer $^{152+154}$Eu(III) was added in the polyethylene tubes to achieve the desired concentrations. The pH values were adjusted to required value by adding negligible volumes of 0.1 mol/L or 0.01 mol/L $HClO_4$ or NaOH solution. The centrifuge tubes were shaken on a rotating oscillator for 6.0 h to achieve adsorption equilibrium. Afterward, the solid was separated from aqueous solutions by a magnetic process using a permanent magnet.

The concentration of $^{152+154}$Eu(III) in the supernatant was determined by liquid scintillation counting (Packard 3100 TR/AB Liquid Scintillation analyzer, Perkin–Elmer) with an ULTIMA GOLD AB (Packard) Scintillation cocktail. The adsorption percentage (R) of Eu(III) on MFSC was calculated according to the equation of $R(\%) = 100\% \times (1 - A_L/A_{tot})$, where A_L is the activity of $^{152+154}$Eu(III) in supernatant and A_{tot} is that of $^{152+154}$Eu(III) in suspension.

3. Results and discussion

3.1. Characterization of MFSC

The SEM micrographs of pristine sepiolite, defibered sepiolite, and MFSC are illustrated in Fig. 2. Obviously, the fiber clusters of pristine sepiolite (Fig. 2(A)) almost disappear after defibering treatment, and it can be observed that defibered sepiolite (Fig. 2(B)) presents in the form of dispersive fibers with a high length-diameter ratio. Compared with the morphology of defibered sepiolite, noticeable differences can be found in the SEM micrograph of MFSC (Fig. 2(C) and (D)), which can be illustrated from the Fe_3O_4 nanoparticles covered on the surfaces of defibered sepiolite. Fig. 2(D) shows a relatively high magnification image of MFSC. From Fig. 2(D), one can see that the Fe_3O_4 nanoparticles have a uniform size and are almost evenly distributed on the surfaces of defibered sepiolite. The SEM micrographs prove the successful synthesis of MFSC and indicate that the surface of sepiolite is modified by Fe_3O_4 nanoparticles in the material.

Fig. 3 shows the XRD patterns of pristine sepiolite, defibered sepiolite, and MFSC. The peaks marked by (S, C, T, and M) are the characteristics of sepiolite, calcite, talc-2 M, and magnetite, respectively. The peaks of calcite almost disappear completely in the XRD pattern of defibered sepiolite, indicating that the main impurity calcite in pristine sepiolite is removed effectively. It is obvious that the purity of defibered sepiolite is much higher than pristine sepiolite. Compared with defibered sepiolite, the XRD pattern of MFSC displays five new peaks at 30.1˚, 35.5˚, 43.3˚, 57.2˚, and 62.7˚, which can be assigned to the characteristic peaks of cubic magnetite phase (JCPD No. 89-3854). Besides, the characteristic peaks of sepiolite in the XRD pattern of MFSC weaken obviously, indicating that the structure of sepiolite may be partly destroyed resulting in confusional crystal lattice [17].

Fig. 4 describes the FT-IR spectra of pristine sepiolite, defibered sepiolite, and MFSC. The bands in the FT-IR spectrum of defibered sepiolite may be summarized as follows: (I) the band at 3,686 cm^{-1} corresponds to the triple bridge group Mg_3OH; (II) the stretches at 3,425 cm^{-1} and the –OH bending mode at 1,669 cm^{-1} are associated with zeolitic water; (III) bands in the range of 1,200–400 cm^{-1} are characteristic of silicate, that is, bands centered at 1,025 and 465 are

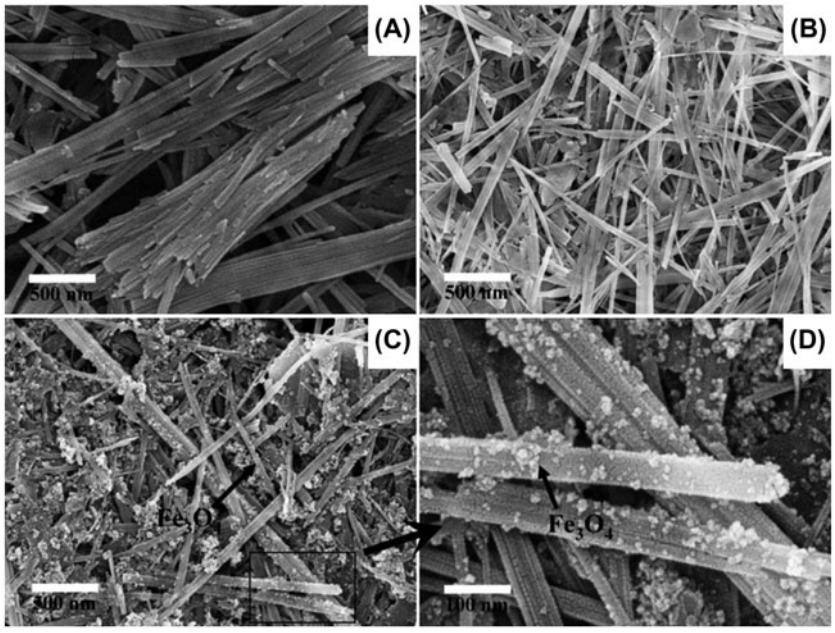

Fig. 2. SEM images of pristine sepiolite (A), defibered sepiolite (B), and MFSC ((C) and (D)).

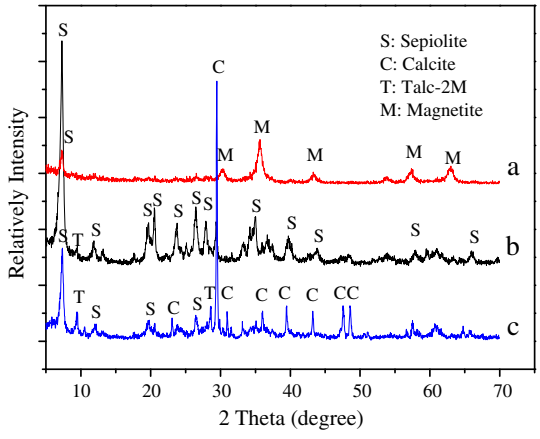

Fig. 3. XRD patterns of MFSC (a), defibered sepiolite (b), and pristine sepiolite (c).

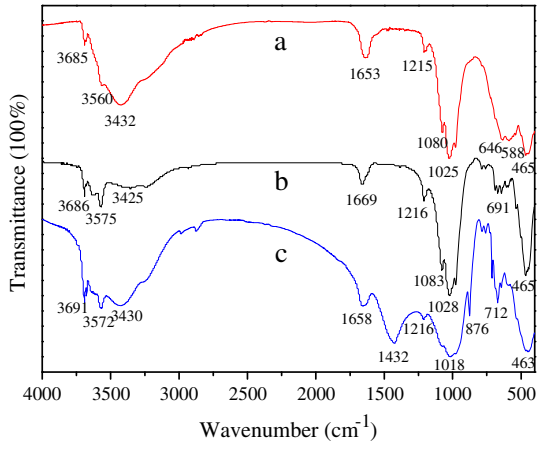

Fig. 4. FT-IR spectra of MFSC (a), defibered sepiolite (b), and pristine sepiolite (c).

due to Si–O–Si vibration and bands at 1,216, 1,083 cm^{-1} are due to Si–O bonds [18]. For pristine sepiolite, the bands at 1,432, 876, and 712 cm^{-1} correspond to the stretching vibration peaks of CO_3^{2-} [19], it is noticeable that the three peaks disappear in the FT-IR spectrum of defibered sepiolite, indicating that the impurity calcite has been effectively removed after purification. As the defibered sepiolite alters to MFSC, changes in the defibered sepiolite adsorption bands of the sample are noted at 3,686, 3,575, and 691 cm^{-1}. The band at 3,575 cm^{-1} is replaced by a broad band at 3,432 cm^{-1}, which is due to stretching vibrations of hydroxyl groups from Fe_3O_4 and water [20]. In addition, the band at 588 cm^{-1} corresponds to the characteristic stretching vibration of the Fe–O bond, which demonstrates the presence of Fe_3O_4 nanoparticles. The assignments of the peaks observed are shown in Table 1.

N_2 adsorption–desorption isotherms and corresponding Barrett, Joyner, and Halenda (BJH) pore-size distribution curves of defibered sepiolite and MFSC are shown in Fig. 5. It is found that the isotherms for N_2 are type I for defibered sepiolite and MFSC in the

Table 1
Peak assignments of pristine sepiolite, defibered sepiolite, and MFSC

Band position (cm^{-1})	Assignments
3,691, 3,686, 3,685	MgOH (trioctahedral) stretch
3,572, 3,575, 3,560	OH-stretch from coordinated water
3,432, 3,430, 3,425	Water OH stretch, FeOH stretch
1,669,1,658,1,653	Water OH bend
1,432	Calcium carbonate impurity
1,216, 1,215	SiOH stretch
1,083, 1,080	SiOH stretch
1,028, 1,025, 1,018	SiOH stretch
876	Calcium carbonate impurity
712	Calcium carbonate impurity
691	OH translation
646	OSiO bends
588	Fe–O stretch
465, 463	OSiO bends

IUPAC classification [21], suggesting that defibered sepiolite and MFSC belong to typical microporous materials. The N_2-BET specific surface areas of defibered sepiolite and MFSC are measured to be 116.43 and 106.33 m^2/g, respectively. The average pore sizes for defibered sepiolite and MFSC are 13.12 and 11.30 nm, respectively, with a wide distribution of pore size. The results indicate that both the specific surface area and average pore size of MFSC decrease slightly after Fe_3O_4 nanoparticles coating on the surface of sepiolite.

The magnetization property of MFSC was investigated at room temperature by measuring magnetization curves (Fig. 6). Fig. 6 shows the superparamagnetic property of MFSC and the saturation magnetization, M_s, of MFSC is about 16.85 emu/g, indicating that MFSC has a high magnetism. Fig. 7 shows photographs of the magnetic separation process of MFSC. MFSC can be dispersed in double distilled water by sonicating for 1 min. As a permanent magnet was used to approach the glass vial containing MFSC dispersed double distilled water, the particles of MFSC are attracted toward the magnet very quickly (within 5 min) and accumulated to the side of glass vial, leaving the aqueous solutions clear and transparent. However, the defibered sepiolite in the glass vial maintains the original dispersive institutions and cannot be attracted by the external magnetic field. The easy and highly efficient magnetic separation process demonstrates that the synthesized MFSC can be used as a magnetic adsorbent in metal ion pollution management.

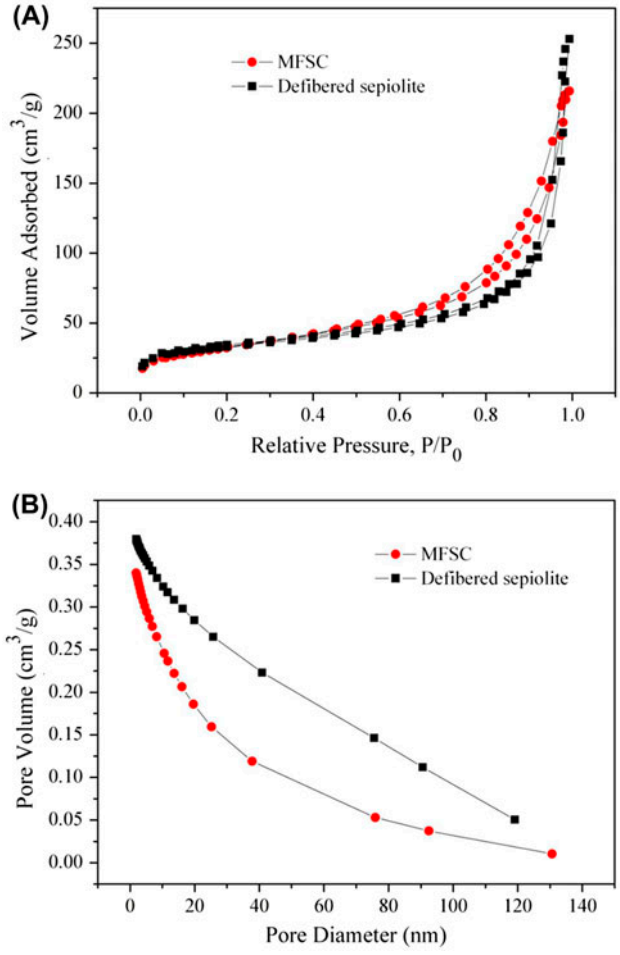

Fig. 5. N_2 adsorption–desorption isothermal curves (A) and corresponding BJH poresize distribution curves (B) of defibered sepiolite and MFSC, the pore-size distribution was calculated from the desorption branch of the isotherm.

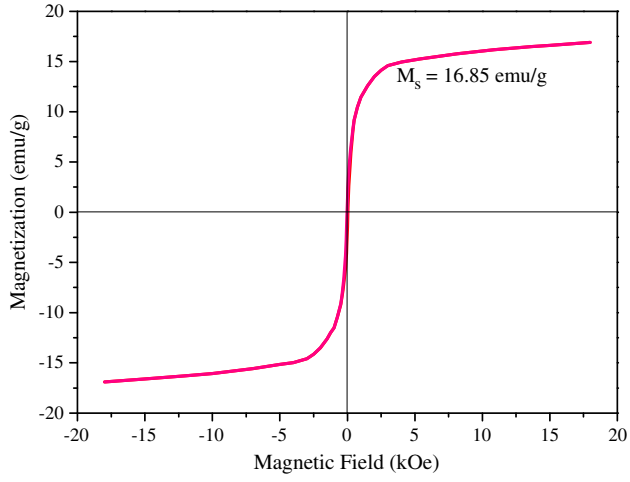

Fig. 6. Magnetization curve of MFSC at room temperature.

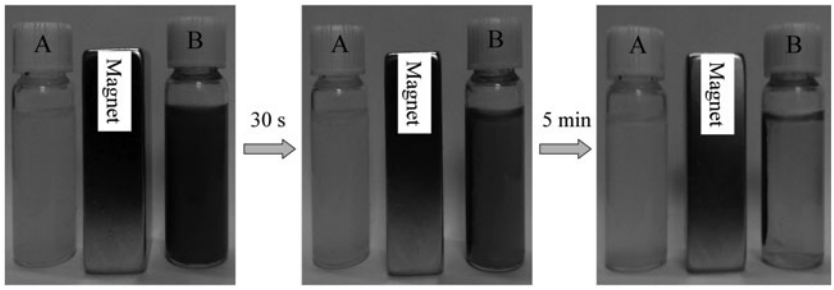

Fig. 7. Photographs of the magnetic separation processes of defibered sepiolite (A) and MFSC (B).

3.2. Effect of pH and ionic strength

Solution pH governs the speciation of metals and also the dissociation of active functional sites on the adsorbent [22]. It has been considered to be the most important variable affecting metal adsorption on the adsorbent, this can be partly attributed to the strongly competitive effects between hydrogen ions and adsorbate [23]. In view of this point, the adsorption of Eu (III) on MFSC as a function of pH was investigated in 0.001, 0.01, and 0.1 mol/L $NaClO_4$ solutions, respectively. As shown in Fig. 8, the removal percentage of Eu(III) in 0.01 mol/L $NaClO_4$ solution increases gradually from ~10 to ~90% as pH increases from 2.0 to 7.0, and then maintains at an aptotic value (~95%) with increasing pH. The result is similar to that of Eu(III) in mesoporous molecular sieve as a function of pH values [14].

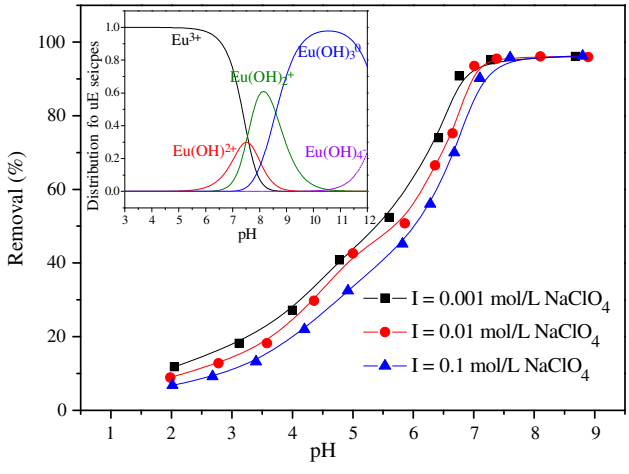

Fig. 8. Effects of pH and ionic strength on the adsorption of Eu(III) on MFSC and relative proportion of Eu(III) species as a function of pH (inset).
Notes: $C_{Eu(III)initial}$ = 15.0 mg/L, m/V = 0.5 g/L, T = 293 ± 1 K, I = 0.01 mol/L $NaClO_4$.

The observed removal trends are related with the surface properties of MFSC and the distribution of Eu (III) species in solution. Since there is a great number of silanol groups and hydroxyl groups in the external surfaces of sepiolite and Fe_3O_4 nanoparticles, the hydroxyl groups on the surfaces of MFSC (≡XOH, where ≡X represents the surface of MFSC, and –OH represents the oxygen-containing functional groups) can be considered as the surface complexation site. The surface of MFSC is positively charged at low pH due to the protonation of reaction on the surfaces (i.e. $H^+ + \equiv XOH \rightarrow \equiv XOH_2^+$). The low removal percentage is attributed to the electrostatic repulsion occurred between metal ion and the edge groups with positive charge (XOH_2^+) on the surface of MFSC. At high pH, the surface is of negatively charged due to the deprotonation reaction ($\equiv XOH \rightarrow \equiv XO^- + H^+$) and electrostatic repulsion decreases with increasing pH due to the reduction of positive charge density on the edges, which enhances the removal of the positively charged Eu(III) ions through electrostatic force of attraction. In addition, more surface functional groups are dissociated at high pH values than that at low pH values, which provides more available sorption sites and therefore causes higher Eu(III) removal.

According to the hydrolysis constants of Eu(III) listed in Table 2 [13], the relative distribution species of Eu(III) in 0.01 mol/L $NaClO_4$ solution as a function of pH are shown in the inset of Fig. 8. It is obviously that Eu^{3+} is dominated at pH < 6.0, and the removal

Table 2
Eu(III) hydrolysis reactions and equilibrium constants [13]

Reactions	Log K
$Eu^{3+} + H_2O \leftrightarrow Eu(OH)^{2+} + H^+$	−7.64
$Eu^{3+} + 2H_2O \leftrightarrow Eu(OH)_2^+ + 2H^+$	−15.1
$Eu^{3+} + 3H_2O \leftrightarrow Eu(OH)_3^0 + 3H^+$	−23.7
$Eu^{3+} + 4H_2O \leftrightarrow Eu(OH)_4^- + 4H^+$	−36.2

of Eu(III) is mainly accomplished via outer-sphere complexation and ion-exchange process in the pH range. The process can be expressed as follows [15,24,25]:

$$\equiv XOH + Eu^{3+} \rightarrow \equiv XOHEu^{3+} \quad (1)$$

$$3 \equiv XOH + Eu^{3+} \rightarrow (\equiv XO)_3Eu + 3H^+ \quad (2)$$

While at pH > 6.0, hydroxides $Eu(OH)_2^+$, $Eu(OH)_2^+$ and $Eu(OH)_3$ become predominantly, and the inner-sphere complexation and surface precipitation become predominant. This can be explained by the following reactions:

$$\equiv XO^- + Eu^{3+} \rightarrow \equiv XOEu^{2+} \quad (3)$$

$$2(\equiv XO^-) + Eu^{3+} \rightarrow (\equiv XO)_2Eu^+ \quad (4)$$

$$2(\equiv XO^-) + Eu^{3+} + H_2O \rightarrow (\equiv XO)_2EuOH + H^+ \quad (5)$$

$$Eu^{3+} + 3H_2O \rightarrow Eu(OH)_{3(s)} + 3H^+ \quad (6)$$

The effect of ionic strength on Eu(III) removal as a function of pH is also shown in Fig. 8. One can see that Eu(III) removal is affected obviously by ionic strength at pH < 7.0, and no effect is found at >7.0. Outer-sphere surface complexes are expected to be more impressionable to ionic strength variations than inner-sphere complexes as the background electrolyte ions are placed in the same plane for outer-sphere surface complexes [26]. From the above discussion, it is plausible that ion exchange and outer-sphere surface complexation mainly contribute to Eu(III) removal on MFSC at pH < 7.0, while inner-sphere surface complexation and precipitation is the main mechanism of Eu(III) removal on MFSC at pH > 7.0 [27].

3.3. Adsorption kinetic study

The effect of contact time on the adsorption of Eu (III) by MFSC is illustrated by Fig. 9. The regularity for Eu(III) adsorption between the two different initial Eu(III) concentration as a function of contact time is similar. The adsorption capacity of Eu(III) increased rapidly at the initial stage of adsorption. Maximum adsorption was reached within 3 h for Eu(III); thereafter, the adsorption capacity increased slowly and reached completely equilibrum at 6 h. The quick adsorption of Eu(III) on MFSC suggests that chemical

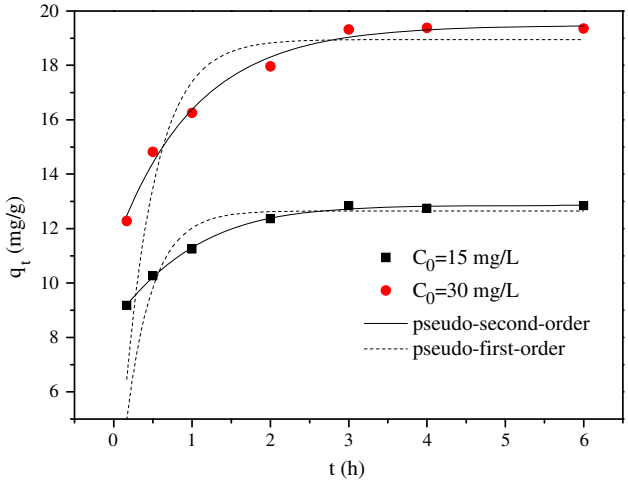

Fig. 9. Adsorption of Eu(III) on MFSC as a function of contact time.
Notes: pH = 5.00 ± 0.05, m/V = 0.5 g/L, T = 293 ± 1 K, I = 0.01 mol/L $NaClO_4$.

adsorption rather than physical adsorption contributes Eu(III) adsorption on MFSC surface [28].

In order to analyze the adsorption rate of Eu(III) on MFSC, two common kinetic models (pseudo-first-order and pseudo-second-order) were applied to simulate the kinetic adsorption. The pseudo-first-order equation is expressed as [29]:

$$\frac{dq_t}{dt} = k(q_e - q_t) \quad (7)$$

After integration, the linear form of Eq. (7) becomes:

$$\ln(q_e - q_t) = \ln q_e - kt \quad (8)$$

where q_t (mg/g) is the amount of Eu(III) adsorbed on MFSC at time t (h), q_e (mg/g) is the adsorption capacity at equilibrium, and k is the rate constant of the pseudo-first-order sorption (h^{-1}).

The pseudo-second-order equation can be expressed as following formulation [30]:

$$\frac{t}{q_t} = \frac{1}{Kq_e^2} + \frac{1}{q_e}t \quad (9)$$

where K (g/(mg h)) is the pseudo-second-order rate constant.

Fig. 9 illustrates the comparative results of the two kinetic models and Table 3 lists the adsorption equilibrium and rate constants. For the two applied kinetic

Table 3
Kinetic parameters for the adsorption of Eu(III) on MFSC at different concentrations

Adsorbate concentration (mg/L)	Pseudo-first-order model			Pseudo-second-order model		
	k (h^{-1})	q_e (mg/g)	R^2	K (g/mg/h)	q_e (mg/g)	R^2
C_0 = 15	0.893	12.88	0.841	0.660	13.12	0.999
C_0 = 30	0.774	18.90	0.793	0.306	19.95	0.998

models, one can see that the pseudo-second-order model fitted the adsorption data better than pseudo-first-order model from the fitting curves shown in Fig. 9 and the correlation coefficients shown in Table 3.

3.4. Adsorption isotherms

Adsorption isotherms of Eu(III) adsorption on MFSC obtained at 293, 313, and 333 ± 1 K are shown in Fig. 10. With Eu(III) concentration increasing, the adsorption increases gradually. This could be explained by the fact that increasing metal concentration in the aqueous solutions may enhance the contacting probability between metal ions and adsorbent surface. Adsorption isotherms become higher in the order of 293, 313, and 333 ± 1 K, suggesting that the adsorption process is favored at high temperatures.

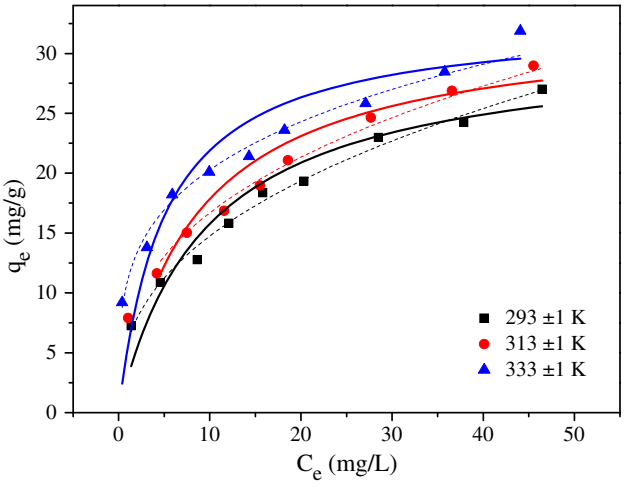

Fig. 10. Adsorption isotherms of Eu(III) adsorption on MFSC at different temperatures.
Notes: Symbols denote experimental data, solid lines represent the model fitting of Langmuir equation, and dashed lines represent the model fitting of Freundlich equation; pH = 5.00 ± 0.05, m/V = 0.5 g/L, $C_{Eu(III))initial}$ = 5–60 mg/L, I = 0.01 mol/L $NaClO_4$.

The Langmuir and Freundlich models are used most commonly to describe the adsorption characteristics of adsorbent. The Langmuir isotherm model is commonly used to describe monolayer adsorption process onto surfaces. Its form can be expressed by the following equation [31]:

$$C_e/q_e = 1/K_L q_m + C_e/q_m \quad (10)$$

where q_m (mg/g), the maximum adsorption capacity, is the amount of adsorbate at complete monolayer coverage, q_e (mg/g) is the equilibrium adsorption capacity, and K_L (L/mol) is the Langmuir constant that relates to the heat of adsorption.

The Freundlich isotherm model is an empirical relationship describing the adsorption of solutes from a liquid to a solid surface, and assumes that different sites with several adsorption energies are involved. The model can be represented by the following equation [32]:

$$\log q_e = \log K_F + n \log C_e \quad (11)$$

where K_F ($mg^{1-n}\,L^n/g$) is roughly an indicator of the adsorption capacity and n is the degree of heterogeneity of adsorbent. The Freundlich parameters (K_F and n) indicate whether the nature of adsorption is either favorable or unfavorable.

The relative values (K_L, q_m, K_F, and n) calculated from the two models are listed in Table 4. From the fitting curves in Fig. 10 and the correlation coefficients (R^2) listed in Table 4, it is clear that the Freundlich model fits the adsorption data better than the Langmuir model. It is generally regarded that the Langmuir isotherm model is valid for dynamic equilibrium adsorption process on completely homogenous surfaces, whereas the Freundlich isotherm model is applicable to heterogeneous surface. The result found in this work was identical to that reported in the reference of [25], which showed that the adsorption of Eu (III) on attapulgite can be fitted by Freundlich model better than Langmuir model.

Table 4
Parameters for Langmuir and Freundlich models of Eu(III) adsorption on MFSC

Experimental conditions (K)	Langmuir			Freundlich		
	q_{max} (mg/g)	b (L/mg)	R^2	K_F (mg^{1-n} L^n/g)	n	R^2
T = 293 ± 1	30.85	0.105	0.967	6.17	0.381	0.989
T = 313 ± 1	32.72	0.134	0.969	7.38	0.354	0.992
T = 333 ± 1	33.88	0.198	0.964	11.14	0.260	0.985

3.5. Comparison of Eu(III) adsorption with other adsorbents and reusability

In order to verify the feasibility of using MFSC as a potential adsorbent for radioactive wastewater disposal, the maximum adsorption capacity (i.e. q_{max} obtained from Langmuir model fitting) of MFSC toward Eu(III) was carefully compared with those reported in previous literature [11–13,33–40]. The values of adsorption capacities are presented in Table 5. The results showed that MFSC has a high adsorption capacity for Eu(III) as comparable with that of other adsorbents except activated carbon and graphene oxide. However, activated carbon and graphene oxide are not able to support wide application, because of their high raw-material cost or high synthetic cost, as well as their potential ecological toxicity. In contrast, the MFSC can be easily synthesized by a simple chemical co-precipitation method. Besides, the MFSC can be easily separated from aqueous solutions in several minutes by a permanent magnet.

In addition, the regeneration and reusability of MFSC through many cycles of sorption/desorption were investigated. Since the iron oxide nanoparticles can be partly degraded at low pH and it can lead to the damage of adsorbent structure, NaOH was used as the strippant to conduct the regeneration operation and the regenerated MFSC was used for six consecutive cycles. The Eu(III)-loaded MFSC was left in contact with 0.05 mol/L NaOH solutions in a solid–liquid ratio of 1.0 g/L. The initial concentration of Eu(III) was chosen to 60.0 mg/L. After shaken for 2.0 h, the sample was separated from the dispersions by a permanent magnet. Fig. 11 shows the relationship between regeneration cycle number and the corresponding adsorption capacity of Eu(III). With increasing cycle number, the adsorption capacity of Eu(III) decreases slightly from 27.02 to 24.80 mg/g. The puny decrease in adsorption capacity is attributed to the incomplete Eu(III) desorption from the surfaces of MFSC [35]. The excellent regeneration property of MFSC suggests that it can be used as a cost-effective material for the removal of Eu(III) from aqueous solutions.

3.6. Adsorption mechanism

In order to further confirm the adsorption mechanism, the FT-IR and XPS analysis were performed and the results are presented in Figs. 12 and 13, respectively. FT-IR spectra of the unloaded and Eu(III)-loaded MFSC

Table 5
Comparison of Eu(III) adsorption capacities of MFSC with that of different adsorbents

Adsorbents	q_{max} (mg/g) (Eu(III))	Experimental conditions	Refs.
ZSM-5 zeolite	3.28	pH 5.0; T 298 K	[11]
Fe_3O_4@HA MNPs	10.56	pH 5.0; T 293 K	[12]
Bare TiO_2	1.51	pH 4.5; T 293 K	[13]
Synthetic saponite	0.71	pH 5.0; T 298 K	[33]
Na-montmorillonite	1.02	pH 5.0; T 298 K	[33]
MWCNTs	1.40	pH 4.5; T 298 K	[34]
GMZ bentonite	5.59	pH 6.2; T 298 K	[35]
Activated carbon	46.50	pH 5.0; T 298 K	[36]
Graphene oxide	161.29	pH 4.5; T 298 K	[37]
γ-Al_2O_3	11.40	pH 6.5; T 293 K	[38]
PANI@GO	250.73	pH 3.0; T 298 K	[39]
PAM/GO	25.28	pH 6.0; T 295 K	[40]
MFSC	30.85	pH 5.0; T 293 K	This work

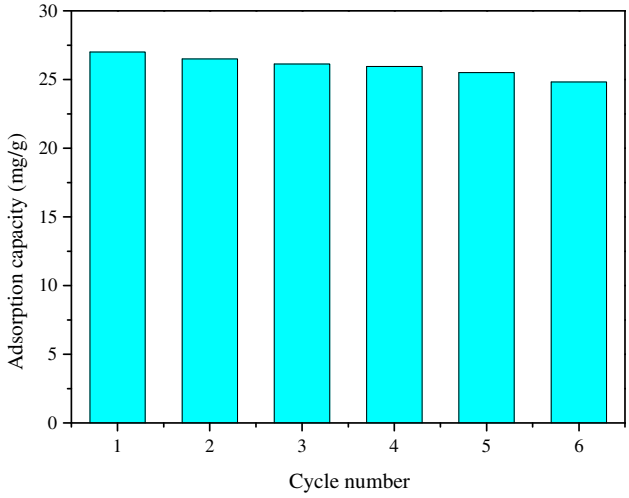

Fig. 11. Recycling of MFSC in the removal of Eu(III).
Notes: pH = 5.00 ± 0.05, $C_{Eu(III))initial}$ = 60 mg/L, T = 293 ± 1 K, m/V = 0.5 g/L, I = 0.01 mol/L $NaClO_4$.

in the range of 400−4,000 cm^{-1} were taken (Fig. 12). Comparison of the spectra presented in Fig. 12 indicates that the intensities of bands at 3,686, 3,432, 1,653, and 646 cm^{-1} weaken significantly for the Eu(III)-loaded MFSC. As mentioned above, the band at 3,686 cm^{-1} is due to the triple bridge group Mg_3OH; the band at 3,432 cm^{-1} corresponds to the stretching vibration of Fe–OH and H–OH; the band at 1,653 cm^{-1} belongs to the bending vibration of –OH, which is associated with zeolitic water; the band at 646 cm^{-1} is assigned to bending vibration of O–Si–O. The intensity decrement of

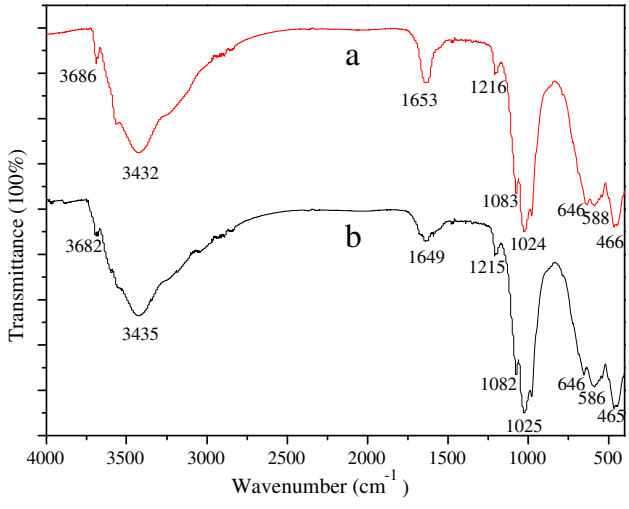

Fig. 12. FT-IR spectra of unloaded MFSC (a) and Eu(III)-loaded MFSC (b).
Notes: (pH = 5.00 ± 0.05, $C_{Eu(III))initial}$ = 15 mg/L, T = 293 ± 1 K, m/V = 0.5 g/L, I = 0.01 mol/L $NaClO_4$.

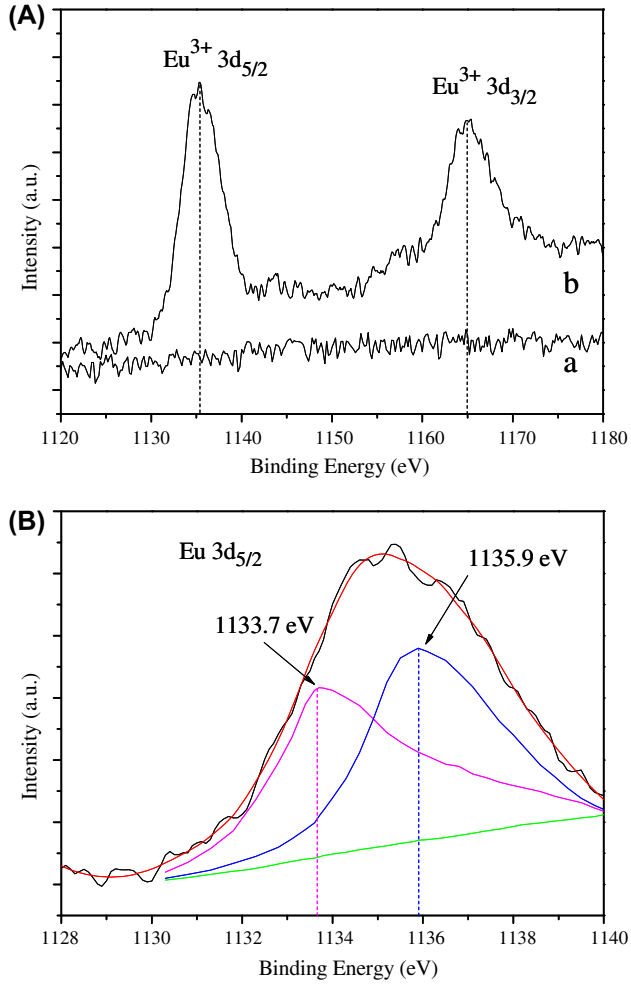

Fig. 13. (A) Eu 3d XPS spectra for unloaded MFSC (a) and Eu(III)-loaded MFSC (b), and (B) The deconvolution of Eu $3d_{5/2}$ spectrum for Eu(III)-loaded MFSC.

bands at 3,686, 3,432, 1,653, and 646 cm^{-1} implies the decrease in triple bridge group Mg_3OH, zeolitic water, Fe–OH, and SiOH in the structure of MFSC [41]. The FT-IR analysis indicates that the Mg_3OH, Fe–OH, and SiOH groups on the surface of MFSC and zeolitic water in the channel of sepiolite mainly involve in the adsorption of Eu(III).

Fig. 13(A) shows the XPS spectra of Eu 3d for unloaded MFSC and Eu(III)-loaded MFSC. Two main peaks, Eu $3d_{5/2}$ at 1,135.3 eV and Eu $3d_{3/2}$ at 1,165.0 eV, with a peak separation of 29.7 eV between the two peaks are observed in Eu(III)-loaded MFSC, whereas no noticeable peaks of Eu 3d are found in unloaded MFSC. The Eu $3d_{5/2}$ core level region spectrum is fitted by deconvolution (Fig. 13(B)). Two peaks at 1,133.7 and 1,135.9 eV are achieved in binary Eu/MFSC system. According to the surface complexation model results, the peaks at 1,133.7 eV may be

assigned to the species of $\equiv SOHEu^{3+}$ and $\equiv X_3Eu^0$, and the peaks at 1,135.9 eV may be attributed to the species of $\equiv SOEu^{2+}$ [13,42–45]. The XPS analysis indicates that surface hydroxyl groups contribute to Eu(III) adsorption to MFSC and surface complexation is one of the main adsorption mechanisms. The results of FT-IR and XPS analysis support the notion that physisorption and chemisorption are involved in the process of Eu(III) adsorption and reveal that ion exchange and surface complexation mainly contribute to Eu(III) adsorption on MFSC.

4. Conclusions

MFSC was synthesized by chemical co-precipitation method and adopted to evaluate its ability to remove Eu(III). The characterization of XRD, FT-IR and N_2 adsorption–desorption showed that the synthesized material was composed of Fe_3O_4 and sepiolite. SEM image of MFSC showed that the surface of sepiolite was uniformly coated by Fe_3O_4 nanoparticles. Furthermore, VSM analysis suggested that MFSC had a superparamagnetic property with the saturation magnetization of 16.85 emu/g, which was high enough to make MFSC be separated from aqueous solutions using an easy magnetic separation method.

The adsorption experiments showed that the removal of Eu(III) on MFSC was highly pH and ionic strength dependent. Adsorption kinetics of MFSC was in good agreement with pseudo-second order. The Freundlich adsorption isotherm provided the better correlation with the adsorption data of MFSC than Langmuir adsorption isotherm. MFSC had a Langmuir adsorption capacity of 30.85 mg/g at 293 ± 1 K, which was much higher than that of some common and low-cost adsorbents. By integrating the FT-IR and XPS analysis, it is plausible that ion exchange and surface complexation mainly contribute to Eu(III) adsorption on MFSC. Considering the good adsorption characteristic, high separation efficiency and excellent regeneration property of MFSC, MFSC is a promising candidate for preconcentration and immobilization of radionuclides from large volumes of aqueous solutions.

Acknowledgment

Financial support from National Natural Science Foundation of China (21277039) is acknowledged.

References

[1] S. Lazarević, I. Janković-Častvan, B. Potkonjak, D. Janaćković, R. Petrović, Removal of Co^{2+} ions from aqueous solutions using iron-functionalized sepiolite, Chem. Eng. Process. 55 (2012) 40–47.
[2] E. Galan, Properties and applications of palygorskite-sepiolite clays, Clay Miner. 31 (1996) 443–453.
[3] S. Kocaoba, Adsorption of Cd(II), Cr(III) and Mn(II) on natural sepiolite, Desalination 244 (2009) 24–30.
[4] S. Lazarević, I. Janković-Častvan, D. Jovanović, S. Milonjić, D. Janaćković, R. Petrović, Adsorption of Pb^{2+}, Cd^{2+} and Sr^{2+} ions onto natural and acid-activated sepiolites, Appl. Clay Sci. 37 (2007) 47–57.
[5] A. Vlad, R. Birjega, A. Matei, C. Luculescu, B. Mitu, M. Dinescu, R. Zavoianu, O.D. Pavel, Retention of heavy metals on layered double hydroxides thin films deposited by pulsed laser deposition, Appl. Surf. Sci. 302 (2014) 99–104.
[6] Y. Zhuang, X.X. Zhao, M.H. Zhou, Cr(VI) adsorption on a thermoplastic feather keratin film, Desalin. Water Treat. 52 (2014) 2786–2791.
[7] M.C. Liu, C.L. Chen, J. Hu, X.L. Wu, X.K. Wang, Synthesis of magnetite/graphene oxide composite and application for cobalt(II) removal, J. Phys. Chem. C 115 (2011) 25234–25240.
[8] C. Daikopoulos, A.B. Bourlinos, Y. Georgiou, Y. Deligiannakis, R. Zboril, M.A. Karakassides, A functionalized phosphonate-rich organosilica layered hybrid material (PSLM) fabricated through a mild process for heavy metal uptake, J. Hazard. Mater. 270 (2014) 118–126.
[9] F.L. Liu, Z.M. Wang, G.Y. Li, Adsorption of Ag^+ by persimmon tannins immobilized on collagen fiber, Desalin. Water Treat. 52 (2014) 7172–7179.
[10] Y.J. Yao, S.D. Miao, S.M. Yu, L.P. Ma, H.Q. Sun, S.B. Wang, Fabrication of Fe_3O_4/SiO_2 core/shell nanoparticles attached to graphene oxide and its use as an adsorbent, J. Colloid Interface Sci. 379 (2012) 20–26.
[11] S.T. Yang, P.F. Zong, X.M. Ren, Q. Wang, X.K. Wang, Rapid and highly efficient preconcentration of Eu(III) by core–shell structured Fe_3O_4@humic acid magnetic nanoparticles, ACS Appl. Mater. Interface 4 (2012) 6891–6900.
[12] D.D. Shao, Q.H. Fan, J.X. Li, Z.W. Niu, W.S. Wu, Y.X. Chen, X.K. Wang, Removal of Eu(III) from aqueous solution using ZSM-5 zeolite, Micropor. Mesopor. Mater. 123 (2009) 1–9.
[13] X.L. Tan, M. Fang, J.X. Li, Y. Lu, X.K. Wang, Adsorption of Eu(III) onto TiO_2: Effect of pH, concentration, ionic strength and soil fulvic acid, J. Hazard. Mater. 168 (2009) 458–465.
[14] L.M. Zuo, S.M. Yu, H. Zhou, J. Jiang, X. Tian, Adsorption of Eu(III) from aqueous solution using mesoporous molecular sieve, J. Radioanal. Nucl. Chem. 288 (2011) 579–586.
[15] D. Xu, Q.L. Ning, X. Zhou, C.L. Chen, X.L. Tan, A.D. Wu, X.K. Wang, Sorption and desorption of Eu(III) on alumina, J. Radioanal. Nucl. Chem. 266 (2005) 419–424.
[16] T. Rabung, H. Geckeis, J.I. Kim, H.P. Beck, The influence of anionic ligands on the sorption behavior of Eu (III) on natural hematite, Radiochim. Acta 82 (1998) 243–248.
[17] S.G. Starodoubtsev, A.A. Ryabova, A.T. Dembo, K.A. Dembo, I.I. Aliev, A.M. Wasserman, A.R. Khokhlov, Composite gels of poly(acrylamide) with incorporated

bentonite. Interaction with cationic surfactants, ESR and SAXS study, Macromolecules 35 (2002) 6362–6369.
[18] A. Tabak, E. Eren, B. Afsin, B. Caglar, Determination of adsorptive properties of a Turkish sepiolite for removal of reactive blue 15 anionic dye from aqueous solutions, J. Hazard. Mater. 161 (2008) 1087–1094.
[19] X.R. Xu, J.T. Han, K. Cho, Formation of amorphous calcium carbonate thin films and their role in biomineralization, Chem. Mater. 16 (2004) 1740–1746.
[20] S. Hsieh, B.Y. Huang, S.L. Hsieh, C.C. Wu, C.H. Wu, P.Y. Lin, Y.S. Huang, C.W. Chang, Green fabrication of agar-conjugated Fe_3O_4 magnetic nanoparticles, Nanotechnology 21 (2010) 445601–445606.
[21] Z.D. Borislav, J.C. Jiří, S. Martin, J. Josef, Pore classification in the characterization of porous materials: A perspective, Cent. Eur. J. Chem. 5 (2007) 385–395.
[22] E. Malkoc, Y. Nuhoglu, Potential of tea factory waste for chromium(VI) removal from aqueous solutions: Thermodynamic and kinetic studies, Sep. Purif. Technol. 54 (2007) 291–298.
[23] Y. Prasanna Kumar, P. King, V.S.R.K. Prasad, Adsorption of zinc from aqueous solution using marine green algae—*Ulva fasciata* sp., Chem. Eng. J. 129 (2007) 161–166.
[24] L.I. Vico, Acid–base behaviour and Cu^{2+} and Zn^{2+} complexation properties of the sepiolite/water interface, Chem. Geol. 198 (2003) 213–222.
[25] L.Q. Tan, Y.L. Jin, X.C. Cheng, J. Wu, W. Zhou, L.D. Feng, Sorption of radioeuropium onto attapulgite: Effect of experimental conditions, J. Radioanal. Nucl. Chem. 290 (2011) 575–585.
[26] C.L. Chen, X.K. Wang, Sorption of Th (IV) to silica as a function of pH, humic/fulvic acid, ionic strength, electrolyte type, Appl. Radiat. Isot. 65 (2007) 155–163.
[27] X.L. Tan, X.K. Wang, H. Geckeis, T.H. Rabung, Sorption of Eu(III) on humic acid or fulvic acid bound to hydrous alumina studied by SEM-EDS, XPS, TRLFS, and batch techniques, Environ. Sci. Technol. 42 (2008) 6532–6537.
[28] X.K. Wang, C.L. Chen, W.P. Hu, A.P. Ding, D. Xu, X. Zhou, Sorption of ^{243}Am(III) to multiwall carbon nanotubes, Environ. Sci. Technol. 39 (2005) 2856–2860.
[29] S. Lagergren, About the theory of so-called adsorption of soluble substances, Kungliga Svenska Vetenskapsakademiens. Handlingar 24 (1898) 1–39.
[30] Y.S. Ho, G. McKay, Pseudo-second-order model for sorption processes, Process Biochem. 34 (1999) 451–465.
[31] I. Langmuir, The adsorption of gases on plane surfaces of glass, mica and platinum, J. Am. Chem. Soc. 40 (1918) 1361–1403.
[32] H.M.F. Freundlich, Über die adsorption in lösungen (Adsorption in solution), Z. Phys. Chem. 57A (1906) 385–470.
[33] T. Okada, Y. Ehara, M. Ogawa, Adsorption of Eu^{3+} to smectites and fluoro-tetrasilicic mica, Clays Clay Miner. 55 (2007) 348–353.
[34] Q.H. Fan, D.D. Shao, J. Hu, C.L. Chen, W.S. Wu, X.K. Wang, Adsorption of humic acid and Eu(III) to multiwalled carbon nanotubes: Effect of pH, ionic strength and counterion effect, Radiochim. Acta 97 (2009) 141–148.
[35] J. Hu, Z. Xie, B. He, G.D. Sheng, C.L. Chen, J.X. Li, Y.X. Chen, X.K. Wang, Sorption of Eu(III) on GMZ bentonite in the absence/presence of humic acid studied by batch and XAFS techniques, Sci. Chin. Chem. 53 (2010) 1420–1428.
[36] H.M.H. Gad, N.S. Awwad, Factors affecting on the sorption/desorption of Eu(III) using activated carbon, Sep. Purif. Technol. 42 (2007) 3657–3680.
[37] Y.B. Sun, Q. Wang, C.L. Chen, X.L. Tan, X.K. Wang, Interaction between Eu(III) and graphene oxide nanosheets investigated by batch and extended X-ray absorption fine structure spectroscopy and by modeling techniques, Environ. Sci. Technol. 46 (2012) 6020–6027.
[38] S.T. Yang, G.D. Sheng, G. Montavon, Z.Q. Guo, X.L. Tan, B. Grambow, X.K. Wang, Investigation of Eu(III) immobilization on γ-Al_2O_3 surfaces by combining batch technique and EXAFS analyses: Role of contact time and humic acid, Geochim. Cosmochim. Acta 121 (2013) 84–104.
[39] Y.B. Sun, D.D. Shao, C.L. Chen, S.B. Yang, X.K. Wang, Highly efficient enrichment of radionuclides on graphene oxide-supported polyaniline, Environ. Sci. Technol. 47 (2013) 9904–9910.
[40] W.C. Song, X.X. Wang, Q. Wang, D.D. Shao, X.K. Wang, Plasma-induced grafting of polyacrylamide on graphene oxide nanosheets for simultaneous removal of radionuclides, Phys. Chem. Chem. Phys. 17 (2015) 398–406.
[41] E. Eren, H. Gumus, N. Ozbay, Equilibrium and thermodynamic studies of Cu(II) removal by iron oxide modified sepiolite, Desalination 262 (2010) 43–49.
[42] D.F. Mullica, C.K.C. Lok, H.O. Perkins, G.A. Benesh, V. Young, The X-ray photoemission spectra of Nd $(OH)_3$, $Sm(OH)_3$, $Eu(OH)_3$ and $Gd(OH)_3$, J. Electron Spectrosc. Relat. Phenom. 71 (1995) 1–20.
[43] F. Mercier, C. Alliot, L. Bion, N. Thromat, P. Toulhoat, XPS study of Eu(III) coordination compounds: Core levels binding energies in solid mixed-oxo-compounds $Eu_mX_xO_y$, J. Electron Spectrosc. Relat. Phenom. 150 (2006) 21–26.
[44] A. Kowal-Fouchard, R. Drot, E. Simoni, N. Marmier, F. Fromage, J.J. Ehrhardt, Structural identification of europium(III) adsorption complexes on montmorillonite, New J. Chem. 28 (2004) 864–869.
[45] Q.H. Fan, X.L. Tan, J.X. Li, X.K. Wang, W.S. Wu, G. Montavon, Sorption of Eu(III) on attapulgite studied by batch, XPS, and EXAFS techniques, Environ. Sci. Technol. 43 (2009) 5776–5782.